Çukurova Üniversitesi
Mühendislik Fakültesi Dergisi
Çukurova University
Journal of the Faculty of Engineering
ISSN: 2757-9255 CİLT/VOLUME: 40 SAYI/ISSUE: 1 MART/MARCH 2025

# Performance Analysis of Additive Manufacturing of Electrodes via Selective Laser Sintering for Green Hydrogen Production

**Fırat EKİNCİ** [1,a], **Mehmet Erman MERT** [2,b], **Hüseyin NAZLIGÜL** [1,c], **Başak DOĞRU MERT** [1,d], **Burak ESENBOĞA** [3,e], **Abdurrahman YAVUZDEĞER** [1,f]

[1]*Adana Alparslan Türkeş Science and Technology University, Engineering Faculty, Department of Energy Systems Engineering, Adana, Türkiye*
[2]*Adana Alparslan Türkeş Science and Technology University, Advanced Technology Research and Application Center, Adana, Türkiye*
[3]*Adana Alparslan Türkeş Science and Technology University, Engineering Faculty, Department of Electrical & Electronics Engineering, Adana, Türkiye*

[a]***ORCID**: 0000-0002-4888-7881; [b]**ORCID**: 0000-0002-0114-8707; [c]**ORCID**: 0000-0003-3037-8568; [d]**ORCID**: 0000-0002-2270-9032; [e]**ORCID**: 0000-0002-7777-259X; [f]**ORCID**: 0000-0001-8058-4672*

**Article Info**
*Received : 18.02.2025*
*Accepted : 25.03.2025*
*DOI: 10.21605/cukurovaumfd.1665920*

**Corresponding Author**
*Hüseyin NAZLIGÜL*
*hnazligul@atu.edu.tr*

**Keywords**
*Hydrogen production*
*Alkaline electrolysis*
*Selective laser sintering*
*Additive manufacturing*
*Wind turbine*

***How to cite:** EKİNCİ, F., MERT, M.E., NAZLIGÜL, H., DOĞRU MERT, B., ESENBOĞA, B., YAVUZDEĞR, A., (2025). Performance Analysis of Additive Manufacturing of Electrodes via Selective Laser Sintering for Green Hydrogen Production. Cukurova University, Journal of the Faculty of Engineering, 40(1), 111-126.*

## ABSTRACT

Standard electrodes have limitations in design flexibility, production time, cost, material waste, and customization. Additive manufacturing overcomes these barriers, offering an efficient, cost-effective, and environmentally friendly approach to manufacturing electrochemical components. This study explores the usability of selective laser sintering for producing electrodes for green hydrogen production, focusing on emergency applications and prototype development. A honeycomb-structured metal cathode for alkaline electrolysis is 3D-printed and tested for tensile strength. Electrochemical methods, including cyclic voltammetry, linear sweep voltammetry, and chronoamperometry, evaluate its catalytic performance against graphite and platinum electrodes. For a 30-minute electrolysis period, the volume of hydrogen gas values for selective laser sintering manufactured cathode electrodes @ 2.4, 2.7, and 3 V are 10.5, 19.75, and 28.5 mL, respectively. Results show superior performance compared to literature. Additionally, wind turbine models (NACA12, NACA15, NACA18) are analyzed for hydrogen production efficiency, with NACA12 proving most effective at moderate to high wind speeds.

# Yeşil Hidrojen Üretimi için Seçici Lazer Sinterleme Yoluyla Elektrotların Eklemeli İmalatının Performans Analizi

**Makale Bilgileri**
*Geliş : 18.02.2025*
*Kabul : 25.03.2025*
*DOI: 10.21605/cukurovaumfd.1665920*

**Sorumlu Yazar**
*Hüseyin NAZLIGÜL*
*hnazligul@atu.edu.tr*

**Anahtar Kelimeler**
*Hidrojen üretimi*
*Alkalin elektroliz*
*Seçici lazer sinterleme*
*Eklemeli imalat*
*Rüzgar türbini*

***Atıf şekli:** EKİNCİ, F., MERT, M.E., NAZLIGÜL, H., DOĞRU MERT, B., ESENBOĞA, B., YAVUZDEĞR, A., (2025). Yeşil Hidrojen Üretimi için Seçici Lazer Sinterleme Yoluyla Elektrotların Eklemeli İmalatının Performans Analizi. Çukurova Üniversitesi, Mühendislik Fakültesi Dergisi, 40(1), 111-126.*

## ÖZ

Standart elektrotlar tasarım esnekliği, üretim süresi, maliyet, malzeme israfı ve özelleştirme açısından sınırlamalara sahiptir. Eklemeli imalat tekniği bu engelleri aşarak elektrokimyasal bileşenlerin üretiminde verimli, uygun maliyetli ve çevre dostu bir yaklaşım sunar. Bu çalışma, acil durum uygulamalarına ve prototip geliştirmeye odaklanarak yeşil hidrojen üretimi için elektrot üretmek amacıyla seçici lazer sinterlemenin kullanılabilirliğini araştırmaktadır. Alkali elektroliz için petek yapılı bir metal katot 3 boyutlu olarak yazdırılır ve çekme dayanımı açısından test edilmiştir. Döngüsel voltammetri, doğrusal tarama voltammetrisi ve kronoamperometri dahil olmak üzere elektrokimyasal yöntemler, grafit ve platin elektrotlara karşı katalitik performansını değerlendirilmiştir. 30 dakikalık bir elektroliz süresi için, seçici lazer sinterleme ile üretilen katot elektrotları için hidrojen gazı hacmi değerleri @ 2,4, 2,7 ve 3 V sırasıyla 10,5, 19,75 ve 28,5 mL'dir. Sonuçlar, literatüre kıyasla üstün performans göstermektedir. Ayrıca, hidrojen üretim verimliliği açısından rüzgar türbini modelleri (NACA12, NACA15, NACA18) analiz edilmiş ve NACA12'nin orta ila yüksek rüzgar hızlarında en etkili olduğu kanıtlanmıştır.

## 1. INTRODUCTION

Renewable energy and hydrogen are crucial to tackling climate change, as both offer sustainable, emission-free solutions to meet our growing energy needs and decarbonize many sectors of the economy [1-3]. The integration of wind energy to produce alkaline hydrogen holds great promise for the future as it enables the effective storage of surplus renewable energy and the provision of a clean and versatile energy carrier, facilitating the transition to a sustainable and decarbonized energy ecosystem [4,5]. The installation of wind powered electrolysis cells is crucial, especially in situations where conventional power plants cannot provide energy during natural disasters such as earthquakes, as they offer a resilient and sustainable solution for continuous energy generation and storage. The biggest bottleneck in the installation of such a system often occurs during the electrolyzer set-up phase due to the challenges of electrode manufacturing, system integration and, if present, additional complexities. Additive manufacturing technology offers a valuable solution in this context. 3D printing simplifies electrode production by enabling the individual and rapid manufacture of complex components, reducing material waste and facilitating on-demand manufacturing, which ultimately optimizes the efficiency and cost-effectiveness of the system [6-13]. The main advantage is that it can be used to manufacture metal electrodes. One advantage of 3D printed metal electrodes is the ability to create complex and personalized electrode designs that improve the performance and efficiency of many electrochemical processes. In addition, the rapid prototyping and iteration capabilities of 3D printing allow for faster creation and improvement of electrode designs. In addition, this method can provide affordable and environmentally friendly solutions for electrode manufacturing while reducing material waste. It offers instant 3D printing and the desired geometry [14-17]. The parameters influencing hydrogen production in alkali electrolysis include electrolyte concentration, temperature, electrode geometry and material selection [18,19]. Fatouh et al [20] focused on evaluating hydrogen production from an alkali electrolyzer under various operating and geometric parameters. The study aims to determine the optimal conditions for efficient hydrogen generation by considering factors such as electrolyte concentration, temperature, electrode shape, and material. The experimental results show that a 26% concentration of KOH electrolyte, a temperature of 70°C, and an input voltage of 11 V lead to the highest hydrogen production rate, with smooth cylindrical aluminum electrodes of larger diameter being the most suitable choice for the electrolyzer operation. The study of Gillespie and Kriek [21] demonstrates the high performance of a membraneless DEFT alkaline electrolyzer, featuring a nickel oxide-coated anodic electrode and pure nickel cathodic electrode, achieving a remarkable current density of 508 mA cm−2 at 2 VDC. While the gas purity in the system is currently limited due to gas/liquid separation constraints, the technology exhibits stable gas purities across various current density levels, showing promise for integration with renewable energy sources. Gonzalez-Buch et al. [22] carried out investigation in which the significance of 3D electrode structure was underlined. Ni and NiMo metallic coatings were electrodeposited onto a stainless steel AISI 304 substrate using a double-template electrochemical process, and their performance as H2-evolving cathodes was assessed in a 30% KOH solution at varying temperatures. Tafel curve analysis indicated that the NiMo-coated electrodes exhibited superior catalytic activity compared to pure Ni electrodes. Literatures have emphasized the importance of 3D geometries structures of electrodes. However, it is widely acknowledged that a major limitation in numerous investigations is that investigations have been conducted with very small electrode geometries on a laboratory scale, and achieving repeatability, especially on surfaces prepared through galvanostatic methods or chemical deposition processes, not always feasible. Consequently, the production of 3D-printed electrodes holds significant importance. It is noteworthy that there is currently a dearth of research in the literature regarding the performance of materials produced using 3D printing technology with metal feedstock in the context of hydrogen gas production through electrolysis in an alkaline environment. In this study, we present Additive Manufacturing as a method of hydrogen production after thoroughly researching it to overcome the shortcomings indicated above. Nevertheless, this domain is of main significance, particularly in the manufacturing of materials in various geometries and alloy-component ratios. It exhibits considerable promise, especially in the context of producing components with specific dimensions and properties for industrial applications.

In present study, electrodes produced using the additive manufacturing method will pave the way to produce electrodes in any desired structure or shape instead of the conventional geometry and shape. In this way, it will open up ways to use hydrogen energy more efficiently. To make the work even more innovative, the honeycomb structure used in recent years has been adopted. The honeycomb- shaped 3D-printed electrode made of a steel alloy was used as the cathode for the alkaline electrolysis system. The behavior of the catalyst was compared with graphite and platinum electrodes using linear voltammetry, cyclic voltammetry

and chronoamperometry, and the hydrogen volume values generated were also compared. Tensile tests were carried out on the samples and compared.

In this study, the feasibility and effectiveness of cathodes produced via additive manufacturing for hydrogen production are explored, with a particular focus on the newly designed 3Dc honeycomb electrodes. The investigation aims to demonstrate that this process is not only viable in experimental settings but also applicable in industrial applications. Wind energy, harvested through vertical axis wind turbines utilizing different NACA airfoil types, was employed to drive hydrogen production. A detailed analysis of power generation at various wind speeds was conducted, and the results were integrated into both experimental and simulation models. By combining expertise from fields such as chemistry, electrical engineering, electronics, and mechanical engineering, this study provides a comprehensive evaluation of additive manufacturing's role in green hydrogen production. This pioneering work highlights the potential for additive manufacturing technologies, particularly with the 3Dc electrodes, to contribute significantly to sustainable energy solutions, especially in wind-powered hydrogen generation systems.

## 2. MATERIAL AND METHOD

### 2.1. Production of Cathode Electrodes and Characterization

3D printed metal production by Additive Manufacturing has advantages over traditional techniques in that it allows for detailed and complicated geometries while decreasing material waste and allowing for more efficient production, customization, and rapid prototyping. The production of electrodes was achieved via BLT A160 3D metal additive manufacturing machine and the electrode's surface area was 341.95 $mm^2$ in Figure 1.

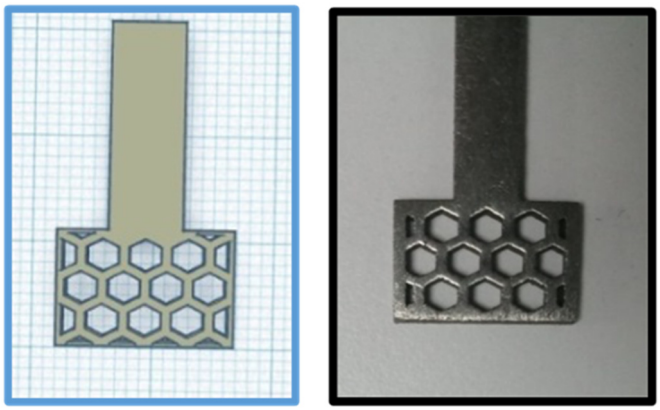

**Figure 1.** The 3Dc (3D metal cathode by Additive manufacturing)

It was denoted as 3Dc (3D manufactured metal cathode). The counter electrode in electrochemical experiments was built of a 1:1:0.01 cm platinum sheet. It also served as the second working electrode for comparison. As a reference electrode, a commercial Ag/AgCl (3 M KCl) was employed. A cylindrical graphite rod with a 0.5 cm diameter served as the third working electrode. The electrochemical tests were achieved in 1 M KOH by galvanostatically using CHI 660B A.C. electrochemical analyser at room temperature, open to atmosphere. The linear sweep voltammetry (LSV) study was carried out using a scan rate of 0.05 V $s^{-1}$. A scan rate of 0.1 V $s^{-1}$ was used for the cyclic voltammetry (CV) investigation. The durability test was performed via chronoamperometry analysis (CA) at -1.8 V. The FEI Quanta 650 Field Emission SEM with an EDX detector was used to get images at 20 keV. The hydrogen gas volume was determined by a two-electrode electrolysis cell which, the Pt was used as anode the working electrode was used as cathode. In the setup of this system, a burette was filled with 1M KOH, it was inverted to the cathode various constant potential values were applied to the system.

The uniaxial tensile experiments of selective 3D printed samples have been performed with a cross-head speed of 1 mm/min on a Shimadzu tensile test machine at room temperature. Each experiment repeated 3 times and the average values were reported as the response variables of the test samples as shown in Figure 2.

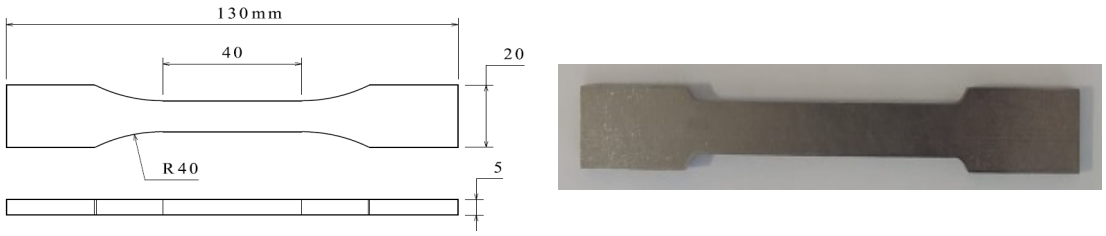


**Figure 2.** The 3D metal printed samples for tensile test

## 2.2. Modeling of a Wind Energy System

The electrolysis process plays an important role in the production of hydrogen by separating water into its components, and this process requires an energy-intensive process. Therefore, using sustainable and renewable energy sources offers great advantages both environmentally and economically. Wind turbines are an ideal option to meet this energy need [23-28]. In particular, using a wind turbine with the appropriate power for electrolysis minimizes the carbon footprint and reduces energy costs by integrating hydrogen production with clean energy. This approach increases the use of renewable energy, reduces fossil fuel dependency and contributes to a more sustainable future. In this study, an optimum wind turbine model is presented for the electrolysis process at different wind speeds.

It is well known that wind and solar energy are among the most studied areas in the literature. Numerous parameters have been examined in studies on these areas of renewable energy. In order to understand the study, the parameters used were as simple and comprehensible as possible. For this reason, simplicity has been prioritized in the simulation studies in the following sections. In this way, the researchers have the opportunity to show the effects of parameters that were not investigated. The wind turbines and hydrogen production through alkaline electrolysis play an important role in sustainable energy production in urban neighborhoods, reducing environmental impact, increasing energy security and facilitating the efficient use of clean energy sources[29–32]. For the wind turbine, the Q-Blade program was used to determine various key parameters that significantly influence the turbine's performance. The program facilitates the estimation of power output, tip speed ratio (TSR) and aerodynamic coefficients such as power coefficient ($C_P$) and lift coefficient ($C_L$). Power output is a key parameter that reflects the turbine's ability to convert wind energy into mechanical power. TSR, which is calculated as the ratio between the tangential speed of the blade tip and the wind speed, is crucial for optimizing the efficiency of the turbine. $C_P$, which represents the efficiency of energy generation, and $C_L$, the lift generated by the blade, are essential factors for evaluating aerodynamic performance.

The performance of turbines used to generate wind energy depends on the type of blades used. These blades have very different numbers and characteristics. For the study presented, a horizontal wind turbine and a suitable blade type studied in the literature were selected for lower energy production and usability. Large wind energy systems are usually installed in remote offshore locations because they require long transmission lines and extensive installation equipment. In contrast, small wind turbines offer advantages in reducing installation costs, especially for modest power generation. When comparing small vertical axis wind turbines (VAWTs) with small horizontal axis wind turbines (HAWTs), VERTs offer significant advantages. This is because HAWTs do not work well in urban areas, which are characterized by high turbulence and low wind speeds. The typically high tip speed ratio of HAWTs results in significant aerodynamic noise from the blades, and the rapid rotation can prevent birds from avoiding them. In contrast, vertical axis wind turbines (VAWTs) typically have a lower tip speed ratio, resulting in less aerodynamic noise. Consequently, VAWTs facilitate the feasibility of wind turbine installations in urban public facilities and residential areas [33-35]. In wind energy simulation studies, the simplest and most useful parameters possible were selected to determine the efficiency of the wind turbine. In wind turbines, the aerodynamic performance of blades is commonly characterized by using the lift coefficient ($C_L$) and drag coefficient ($C_D$). These coefficients elucidate how the blades interact with the airflow, delineating the generation of aerodynamic forces. $C_L$ and $C_D$ values are typically determined through methods such as laboratory tests or computer simulations, and they often exhibit variations for different wind speeds. These coefficients are pivotal parameters for optimizing blade design, ensuring the wind turbine operates with maximum efficiency.

Lift Coefficient ($C_L$)represents the lift force generated by the blades. In wind turbines, the blades exhibit a high-pressure side and a low-pressure side as the airflow passes over them. The $C_L$ coefficient expresses the lift force resulting from this pressure difference. Drag Coefficient ($C_D$) characterizes the resistance force exerted by the blades. When the blades move against the airflow, $C_D$ denotes the resistance force counteracted by the air. $C_L$ and $C_D$ are typically expressed by the following general formulas:

$$C_L = \frac{F_L}{0.5\rho V^2 A} \tag{1}$$

$$C_D = \frac{F_D}{0.5\rho V^2 A} \tag{2}$$

where FL represents the lift force (in Newtons), FD is the drag force (in Newtons), ρ denotes air density (in kilograms per cubic meter), v represents the airspeed (in meters per second). A refers to the wing or surface area (in square meters).

The determination of $C_L$ and $C_D$ values is crucial for advancing the understanding of aerodynamic behavior and optimizing the design of wind turbine blades for enhanced performance [36,37]. The rotor diameter of vertical wind turbines is determined based on various factors and typically varies according to design objectives and application conditions. The rotor diameter directly influences the turbine's ability to capture wind energy and, consequently, mechanical power production. Factors influencing rotor diameter determination include wind speed, power production goals, aerodynamic design, site constraints, cost considerations, and durability. Mechanical power is closely associated with the determined rotor diameter, wind speed, turbine aerodynamic characteristics, and other relevant factors. In this context, mechanical power is often expressed by the following formula:

$$P = \frac{1}{2}\rho A V^3 C_p R\omega \tag{3}$$

where ρ represents the air density, A denotes the turbine blade area, V signifies the wind speed, $C_P$ is the power coefficient, R represents the turbine rotor radius, and ω represents the angular velocity of the turbine. This formula serves as a fundamental mathematical expression for calculating the mechanical power of the turbine. Tip Speed Ratio (TSR) is a crucial parameter in wind turbine design. It represents the ratio between the speed of the tip of the wind turbine blade and the actual wind speed. Wind turbine designers and operators aim to adjust the TSR. A good TSR value depends on various factors, including the specific wind turbine design, site conditions, and the intended purpose of the turbine. TSR selection is crucial for maximizing energy production and ensuring the longevity of wind turbines. TSR is defined as:

$$TSR = \frac{\omega R}{V} \tag{4}$$

where ω is the angular velocity, R is the rotor radius, and V is the wind speed.

## 3. RESULTS AND DISCUSSIONS

Electrolysis requires electrical energy to separate water into hydrogen and oxygen gases, and it is of great importance to meet this energy need in a sustainable manner. Wind turbines, as a renewable energy source, can provide the electrical energy required for the electrolysis process. A wind turbine selected with the appropriate power provides the continuous and sufficient energy required for electrolysis, both increasing operational efficiency and reducing dependency on fossil fuels. In this way, hydrogen production that does not harm the environment and keeps the carbon footprint to a minimum becomes possible. In this study, the hydrogen gas value generated as a result of the electrolysis process will be determined by using the optimum wind turbine model for the electrolysis process. The system design is presented in Figure 3.

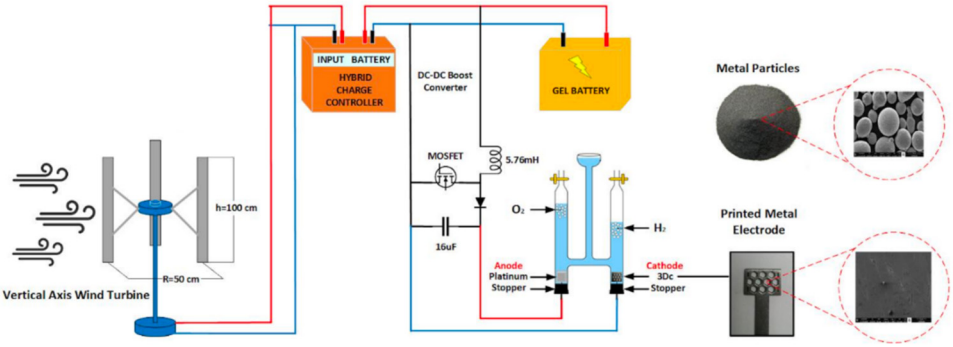


**Figure 3.** Proposed renewable energy-supported electrolysis system

Different wind turbine models are examined for the electrolysis process. The wind turbine model with optimum efficiency is determined for wind turbine models with varying types of blades. The hydrogen production potentials of wind turbine models with electrolysis are compared with different scenarios.

### 3.1. Wind Turbine Models

In order to improve performance of the wind turbine, a vertical axis wind turbine was designed using the Q-Blade program. In order to save cost, the number of blades was reduced on the prototype and the number of blades was selected as three. NACA 0012, NACA0015 and NACA 0018 blades, which are the most preferred blades in the literature, were used in the Q-Blade software to improve the design performance of the vertical axis wind turbine [38–41]. The study focused on power generated by the wind turbine through experimentation with different wind speed and rpm for three airfoil profiles. Figure 4 presents the performance analysis results conducted at different revolutions per minute values and wind speeds ranging from 3 m/s to 18 m/s using NACA 0012, 0015, and 0018 airfoils. These graphs help us understand how wind turbine performance varies with wind speed and rotation speed. Selecting a specific wind speed and rotation speed for optimum power generation can enhance the turbine's efficiency, extend its lifespan, and optimize energy production capacity.

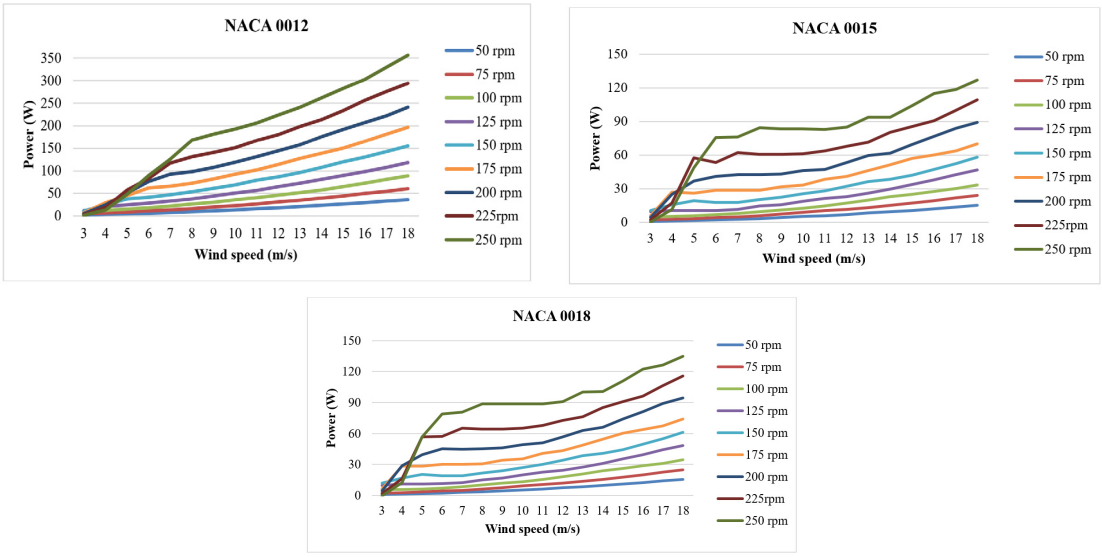


**Figure** 4. Electrical performance at different wind speeds (a) NACA 0012 (b) NACA 0015 (c) NACA0018

Until the wind speed reaches 8 m/s, there is a rapid increase in power production, while after 8 m/s, the increase in power production continues with a less steep slope in Figure 4a. At a wind speed of 18 m/s and a rotation speed of 250 rpm, the power production value reaches 356.9 watts. The steepest points in the power increase for NACA0015 and NACA0018 airfoils are observed at wind speeds of 4 m/s, 5 m/s and 6

m/s, after which it gradually levels off. As seen in Figure 4b and Figure 4c, the maximum power produced is 127.1 watts for NACA0015 and 135 watts for NACA0018, respectively.

The performance assessment of a vertical axis wind turbine, equipped with 3 blades, a rotor diameter of 50 cm, and blade lengths measuring 100 cm, involved experimentation with various airfoils to enhance its efficiency. The performance of a vertical axis wind turbine with three blades, each utilizing a different airfoil, was simulated. The results were presented in Figure 5 for comparative analysis.

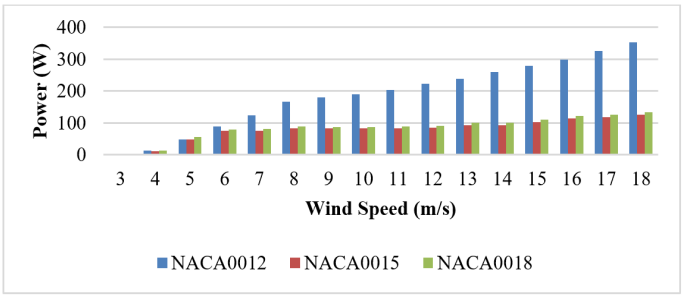


**Figure 5.** The comparison of power generation of wind turbine for airfoils

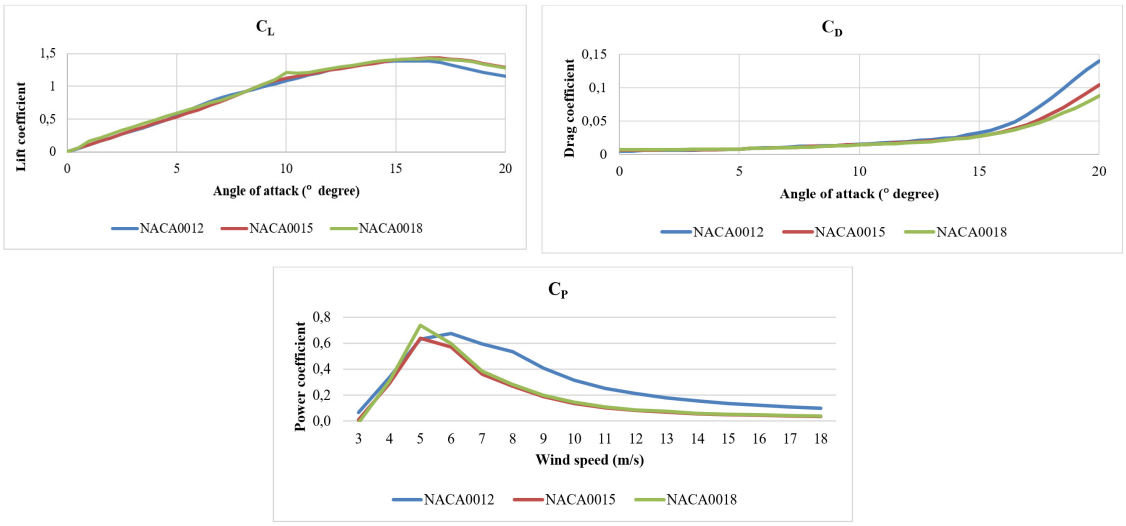


**Figure 6.** The lift coefficients ($C_L$) at angles of attack 0° and 20° (a), The drag coefficients ($C_D$) at angles of attack 0° and 20° (b), The Lift coefficients ($C_P$) from 3 m/s to 18 m/s wind speed (c)

Figure 6a and Figure 6b depict the $C_L$ and $C_D$ values for NAC00A12, NACA0015, and NACA0018 profiles over a range of attack angles from 0° to 20°. As the angle of attack increases from 0°, $C_L$ also increases. At a 15° angle of attack, the NACA12 profile reaches a $C_L$ value of 1.38, indicating that the airfoils are approaching stall. As the angle of attack reaches 20°, $C_L$ decreases to 1.15, signifying that the airfoils have entered the stall. At a 15° angle of attack, NACA0015 and NACA0018 profiles reach a $C_L$ value of 1.4. When the angle of attack reaches 20°, $C_L$ decreases to 1.29 for NACA0015 and 1.28 for NACA0018, respectively.

$C_D$ values increase with the angle of attack as seen Figure 6b. At 20°, NACA0012, NACA0015, and NACA0018 airfoils have $C_D$ values of 0.14, 0.104, and 0.088, respectively. NACA0015 and NACA0018 profiles have a shallower slope angle compared to NACA0012. This results in less lift generated by NACA0015 and NACA0018 profiles. However, the reduced lift also leads to lower drag forces. This enhances the efficiency of the NACA0015 and NACA0018 profiles.

The $C_P$ value in wind turbine blades is the ratio of the power generated by the blades to the power obtained from the wind. Although the highest value is observed in the NACA0018 airfoil at a wind speed of 5 m/s, as the wind speed increases, it can be seen in Figure 6c that the $C_P$ value is much better for NACA0012, and NACA0015 and NACA0018 have approximately the same values.

### 3.2. The Characterization of Electrodes

The morphological characteristics of metal particles pre and post the 3D printing process were scrutinized through Field Emission Scanning Electron Microscopy (FESEM) analysis, and their chemical compositions were ascertained via Energy Dispersive X-ray Spectroscopy (EDX). The corresponding findings were elucidated in Figures 7a and 7b. As depicted in Figure 7a, distinct particle structures were observed, with the particle size falling within the range of 20-50 µm. Furthermore, Figure 7a illustrated the EDX spectra, confirming the presence of Nickel (Ni), Chromium (Cr), Cobalt (Co), Molybdenum (Mo), Manganese (Mn), Aluminum (Al), and Iron (Fe) within the examined metal particles. Figure 7b revealed the presence of homogeneous surfaces. The chemical composition observed on the surface of the 3D-printed sample closely resembled that of the metal particle mixture, indicating a high degree of consistency. When the contents were examined in detail, it was seen that the electrodes produced were compatible with AISI 304 steel.

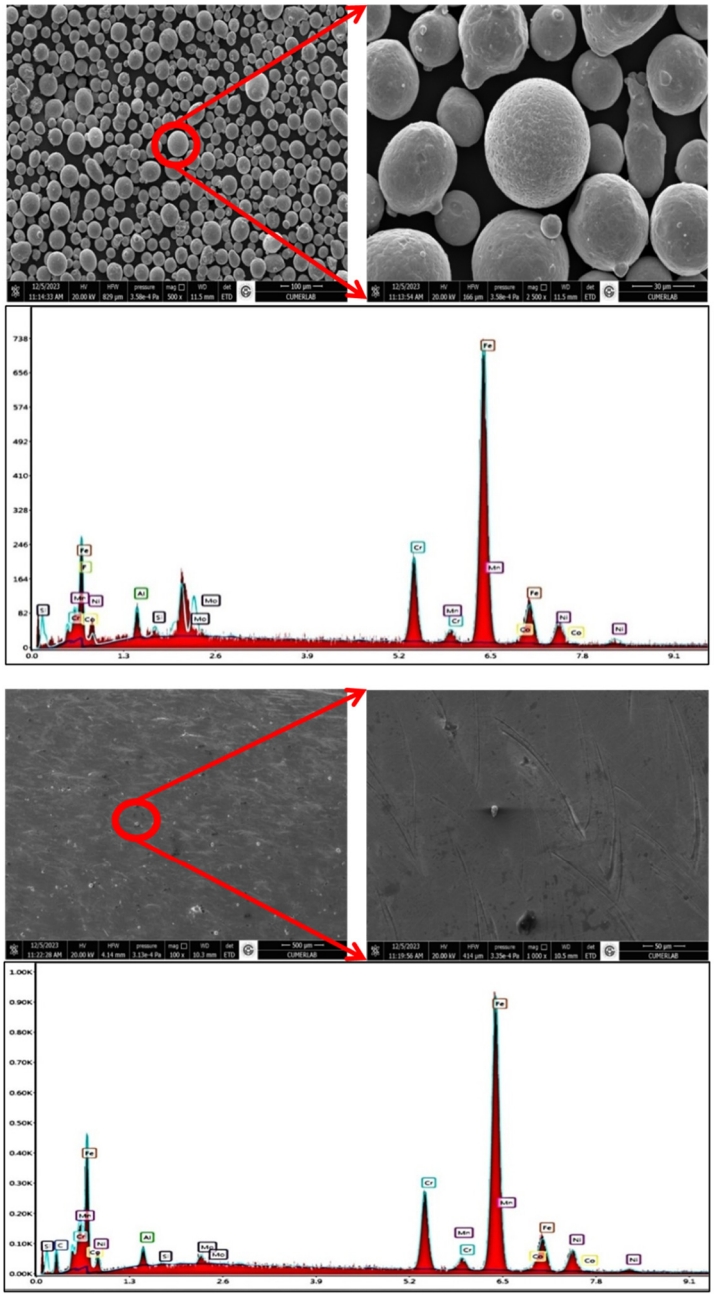

**Figure 7.** The FESEM – EDX measurements of metal particles (a), The FESEM – EDX measurements of 3Dc (b)

Moreover, comparison of the 3D-printed electrode with the properties of AISI 304 steel was substantiated through tensile tests. Three samples for tensile testing were prepared according to ASTM E 8M standards, and the experiments were conducted using a SHIMADZU tensile test machine. The graphical representation of the tensile test results was provided in Figure 8, the results were presented in Table 1. As seen from the analysis result, comparable material was produced via 3D printing method [42,43].

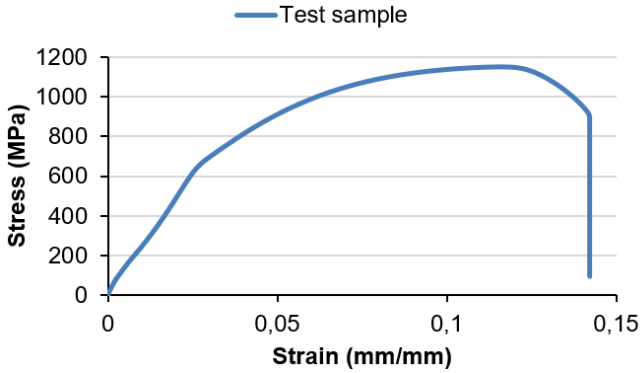


**Figure 8.** Tensile test result of sample

**Table 1.** Investigation and comparison of the properties of test pieces

| | Tensile trength, ultimate (Mpa) | Tensile strength Yield (Mpa) | Elongation at break (%) | Modulus of elasticity (Gpa) | Shear modulus (Gpa) |
|---|---|---|---|---|---|
| **AISI 304** | 505 | 215 | 70 | 193-200 | 86 |
| **AISI 305** | 580 | 230 | 45 | 200 | 77 |

### 3.3. Electrochemical Measurements

The outcomes of the linear sweep voltammetry analysis were depicted in Figures 10 and 11. Evaluation of the hydrogen production efficiency for the examined electrodes centered on their catalytic activity, as indicated by the onset potential and current density values within the cathodic region. Notably, the 3D-printed metal electrode exhibited remarkable effectiveness in comparison to both platinum (Pt) and graphite (G) electrodes among those investigated. This underlined the higher catalytic performance of the 3D-printed electrode than G and comparable with Pt, showcasing its potential as a highly efficient cathode in the context of hydrogen production. The synergistic effects observed in the combination of nickel, cobalt, iron, chromium, and copper showcase a synergistic enhancement of catalytic activity. The concerted action of these metals manifests in improved electronic and structural properties, creating a synergistic environment that elevates the catalytic efficiency for the Hydrogen Evolution Reaction (HER). Particularly, the inclusion of transition metals in the iron electrode induces modifications in its electronic structure, thereby establishing a more favorable energy landscape conducive to the HER. This structural adjustment enhances the adsorption and activation of hydrogen ions, thus facilitating and promoting the reaction. Furthermore, the incorporation of nickel and copper contributes to the generation of additional active sites on the electrode surface. These supplementary active sites play a crucial role in facilitating more hydrogen evolution reactions, so substantially augmenting the overall catalytic activity

The stability of the electrode holds equal importance to its Hydrogen Evolution Reaction (HER) activity. The durability of the electrode during HER is a critical factor as it significantly influences the reliability and reproducibility of experimental outcomes. A durable electrode ensures stable and consistent performance over extended periods, minimizing the necessity for frequent electrode replacements.

The CA analysis results of all electrodes are presented in Figure 9. To assess the electrode's durability, chronoamperometry (CA) technique was employed, followed by immediate Linear Sweep Voltammetry (LSV) measurements presented in Figure 11, and Cyclic Voltammetry (CV) measurements illustrated in Figure 12. These sequential tests provide a comprehensive evaluation of the electrode's stability under prolonged HER conditions, contributing valuable insights into its long-term performance and reliability.

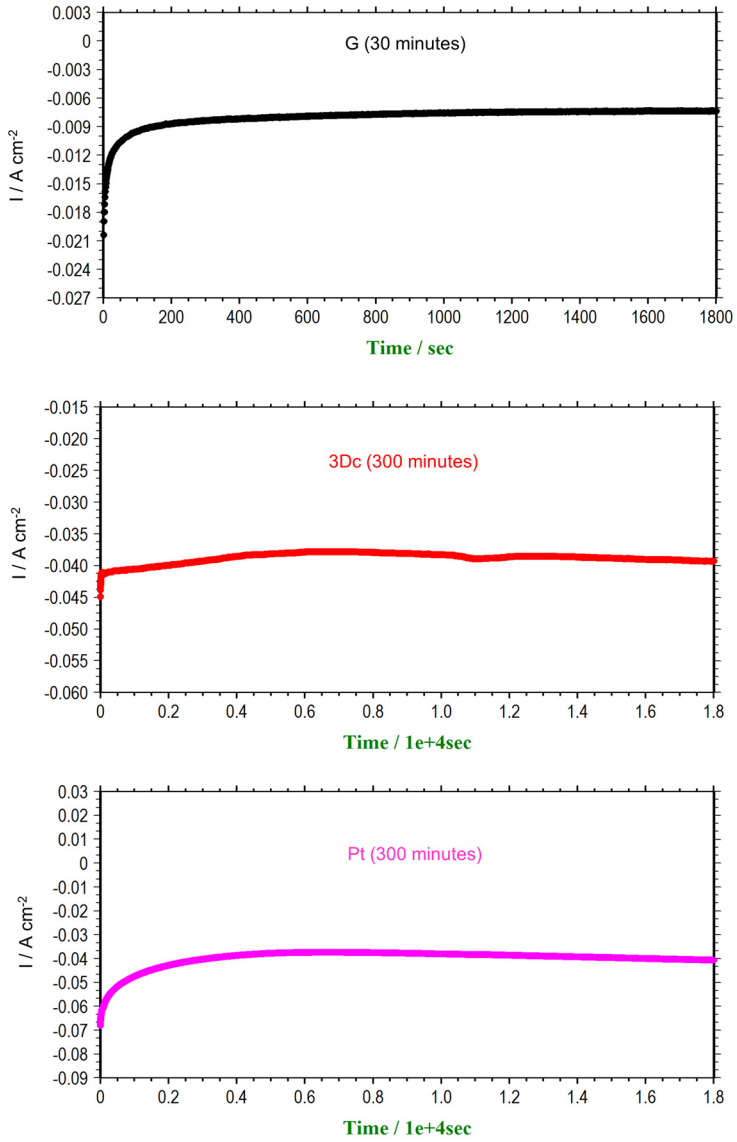


**Figure 9.** The CA analysis of all electrodes

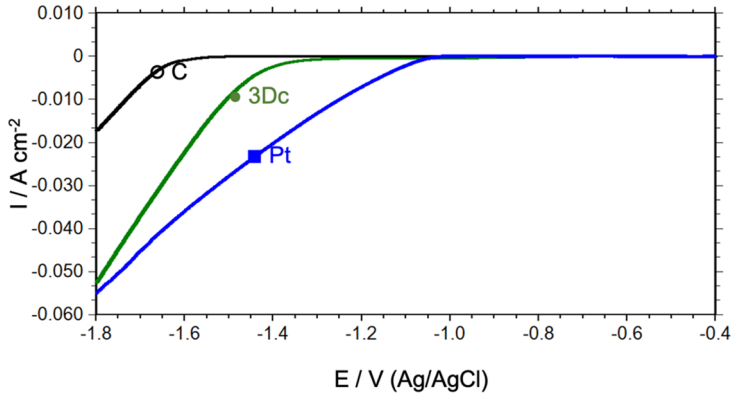


**Figure 10.** The linear sweep voltammograms of C (○), 3Dc (●) and Pt (■) in 1 M KOH solution with scan rate of 50 mV $s^{-1}$

As depicted in Figure 11, according to the results obtained from LSV analysis, it was observed that, following CA analysis (@-1.5V vs Ag/AgCl), G lost its stability, whereas both 3Dc and Pt electrodes maintained their stability.

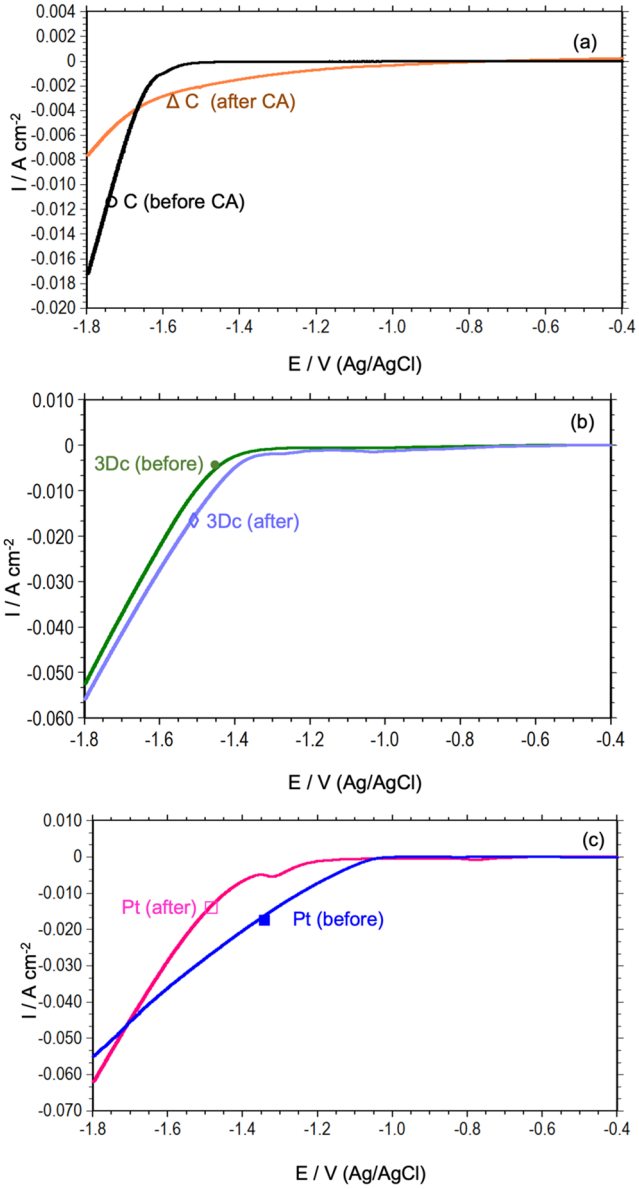


**Figure 11.** The linear sweep voltammograms of electrodes in 1 M KOH solution before and after CA

The 3Dc CV curves before and after CA was shown in Figure 12. After prolonged exposure to cathodic potential, an increase in oxidation current values was observed during subsequent anodic potential scans. This was an anticipated phenomenon in Figure 12.

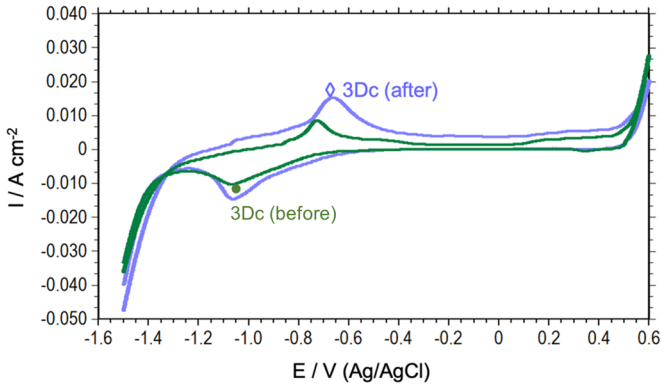


**Figure 12.** The cyclic voltammograms of 3Dc in 1 M KOH solution before and after CA

In Figure 12, the detection of the anodic peak at -0.6 V during forward scanning suggests $Ni/Ni^{2+}$ oxidation, followed by the conversion of $\alpha$-$Ni(OH)_2$ to $\beta$-$Ni(OH)_2$ between -0.4 and 0.4 V (versus Ag/AgCl). $Ni^{2+}/Ni^{3+}$ oxidation is observed around 0.5 V, but $Ni^{3+}/Ni^{2+}$ is identified as a cathodic peak in backward scan at approximately 0.35 V. During the reverse scan, the cathodic peaks were seen in the potential of -1.05 V, related to the reaction of transition metal oxides to reduced forms.

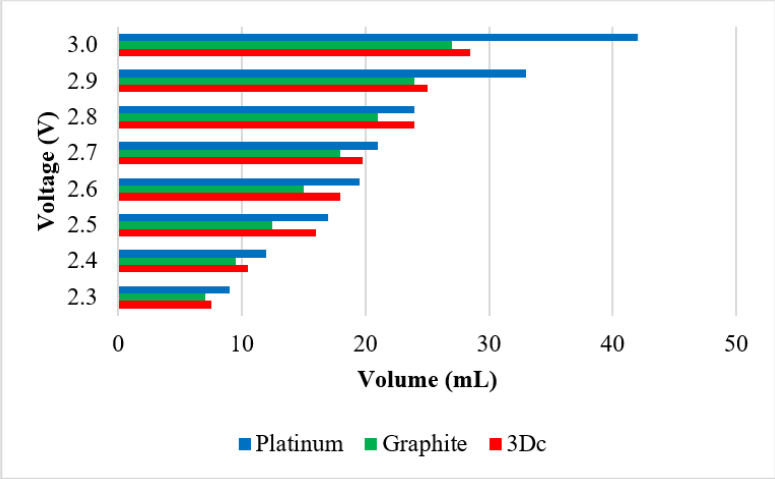


**Figure 13.** Comparison of hydrogen volumes of 3Dc, graphite and platinum electrodes at different voltages during 30 minutes

Figure 13 indicated the volumes of hydrogen produced during the electrolysis process. The production of hydrogen increased gradually with time for each catalyst, positively correlated with the longer electrolysis duration. More hydrogen gas was produced as the potential increased. A volume correction for water vapor was performed to the data collected every five minutes [44]. Additionally, the tests for 3Dc were repeated 3 times and the hydrogen volumes at different voltages for $VH_2$ of 3Dc @ 2.4; 2.7 and 3 V were 10.5; 19.75 and 28.5 mL, respectively for 30 minutes electrolysis period. The 3Dc demonstrated higher hydrogen gas efficiency. The literature comparison showed in Table 2. According to this study, the hydrogen production performance of 3Dc was comparable to that of the literature.

**Table 2.** The hydrogen gas volumes generated during alkaline electrolysis

| Electrodes | Procedures | V $H_2$ (mL) | Ref. |
|---|---|---|---|
| High Carbon Steel | After 30 minutes of electrolysis at a constant potential of 4V | 35.3 | [45] |
| CF/NiGa | After 30 minutes of electrolysis at a constant potential of 3V | 28.9 | [46] |
| C/Ni | After 30 minutes of electrolysis at a constant potential of 3V | 27.7 | [47] |
| C/NiCoW | After 30 minutes of electrolysis at a constant potential of 3V | 30.6 | [47] |
| C/NiCoIr | After 30 minutes of electrolysis at a constant potential of 3V | 29.7 | [47] |
| $Zn_{95}Fe_5$ | After 30 minutes of electrolysis at a constant potential of 5V (0.2 A) | 27 | [48] |
| 3Dc | After 30 minutes of electrolysis at a constant potential of 3V | **28.5** | In this study |

### 3.4. Hydrogen Production Potentials

The analysis of hydrogen production (in liters) from the vertical wind turbine at different wind speeds and NACA airfoil types (NACA12, NACA15, NACA18) demonstrates key differences in performance in Table 3.

**Table 3.** Hydrogen production volumes using the 3Dc electrode in 30 minutes at different wind speeds

| Wind speed (m/s) | NACA12 $H_2$/liter | NACA15 $H_2$/liter | NACA18 $H_2$/liter |
|---|---|---|---|
| **4** | 0.73350333 | 0.62859276 | 0.67811402 |
| **5** | 2.6700771 | 2.69879716 | 3.12643055 |
| **6** | 4.93106704 | 4.18507954 | 4.36531795 |
| **7** | 6.91666556 | 4.2151904 | 4.45993818 |
| **8** | 9.28573644 | 4.67356456 | 4.9028493 |
| **9** | 10.0332071 | 4.6237322 | 4.89097944 |
| **10** | 10.6324492 | 4.61015067 | 4.89155564 |
| **11** | 11.3945096 | 4.59721116 | 4.89676259 |
| **12** | 12.3918196 | 4.70799262 | 5.02394519 |
| **13** | 13.3017033 | 5.19109299 | 5.54816692 |
| **14** | 14.4846031 | 5.19298489 | 5.55387145 |
| **15** | 15.6041429 | 5.75939121 | 6.12762853 |
| **16** | 16.7082088 | 6.36504918 | 6.75359303 |
| **17** | 18.2129725 | 6.56782388 | 6.98919024 |
| **18** | 19.7236072 | 7.02247209 | 7.45757097 |

At low wind speeds (4-6 m/s), the hydrogen production for all three airfoil types is moderate but shows discernible trends. NACA12 produces the highest amount of hydrogen (0.73 liters at 4 m/s), followed closely by NACA18 (0.68 liters), while NACA15 produces the least (0.63 liters). However, at 6 m/s, NACA18 takes the lead with 3.12 liters of hydrogen, surpassing both NACA12 and NACA15. This shift indicates that NACA18 begins to outperform the others as the wind speed increases slightly.

In the mid-range wind speeds (7-10 m/s), NACA12 demonstrates superior performance, generating the most hydrogen consistently across these wind speeds. For example, at 9 m/s, NACA12 produces 10.03 liters of hydrogen, while NACA18 produces 4.89 liters, and NACA15 slightly lags behind. This showcases the efficiency of NACA12 in converting wind energy into hydrogen production more effectively than the other airfoils at these wind speeds.

At higher wind speeds (11-18 m/s), NACA12 continues to dominate in hydrogen production, reaching 19.72 liters at 18 m/s. NACA18 shows strong potential, improving significantly as wind speeds rise, with 7.45 liters of hydrogen produced at 18 m/s. NACA15, while still lower than the other two, begins to show steady growth, producing 7.02 liters at 18 m/s, indicating that it performs better as wind speeds reach their upper range.

Across all wind speeds, NACA12 stands out as the most efficient airfoil for hydrogen production, showing consistent dominance from low to high wind speeds. NACA18 shows a strong ability to catch up at higher wind speeds, indicating it may be better suited for conditions where wind speeds are consistently higher. NACA15, while performing lower across most wind speeds, displays stable increases in hydrogen production as wind speeds increase, indicating that it might be better suited for environments with higher and steadier wind conditions.

## 4. CONCLUSIONS

In this study, a detailed study was carried out for the electrode produced by the 3D additive manufacturing method in hydrogen production. For hydrogen production, different wind turbines were examined. The chemical and mechanical properties of the produced 3D metal printed electrode were investigated and the test results proved its compatibility with AISI 304 steel. The 3D-printed metal electrode outperformed the typical graphite electrode in terms of catalytic efficiency; it lagged behind the platinum electrode, but the results were comparable especially according to price. The VH2 of 3Dc @ 2.4; 2.7 and 3 V were 10.5; 19.75 and 28.5 mL, respectively for 30 30-minute electrolysis period. The 3Dc demonstrated higher hydrogen gas efficiency. The results indicated that 3Dc has the potential to be an efficient cathode for

hydrogen production. The synergistic effects observed from the combination of transition metals contributed to increased catalytic activity, while the electrode's stability, as assessed by chronoamperometry and cyclic voltammetry tests, emphasized its reliability and long-term performance in the hydrogen evolution reaction. These findings illustrated the potential benefits of using such unique electrode designs in sustainable hydrogen production systems. Also, the evaluation of hydrogen production in liters from a vertical wind turbine, considering various wind speeds and different NACA airfoil types, highlights significant differences in performance. In the future, we aim to modify the metal powder by green chemistry methods and the 3D metal printing technology by changing all additive manufacturing parameters that will apply to the production of electrodes.

## 5. ACKNOWLEDGEMENTS

The authors would like to acknowledge the Gokhan PARSAK and PETKA MOLD IND. AND TRADE Inc. for additive manufacturing process.

## 6. REFERENCES

**1.** Al-Orabi, A.M., Osman, M.G. & Sedhom, B.E. (2023). Analysis of the economic and technological viability of producing green hydrogen with renewable energy sources in a variety of climates to reduce CO2 emissions: A case study in Egypt. *Applied Energy, 338,* 120958.

**2.** Liu, J., Zhou, Y., Yang, H. & Wu, H. (2022). Net-zero energy management and optimization of commercial building sectors with hybrid renewable energy systems integrated with energy storage of pumped hydro and hydrogen taxis. *Applied Energy, 321,* 119312.

**3.** Hurtubia, B. & Sauma, E. (2021). Economic and environmental analysis of hydrogen production when complementing renewable energy generation with grid electricity. *Applied Energy, 304,* 117739.

**4.** Qiu, R., Zhang, H., Wang, G., Liang, Y. & Yan, J. (2023). Green hydrogen-based energy storage service via power-to-gas technologies integrated with multi-energy microgrid. *Applied Energy, 350,* 121716.

**5.** Williams, L. & Wang, Y. (2024). A distributed renewable power system with hydrogen generation and storage for an island. *Applied Energy, 358,* 122500.

**6.** Dwivedi, S., Dixit, A.R., Das, A.K. & Nag, A. (2023). A novel additive texturing of stainless steel 316l through binder jetting additive manufacturing. *International Journal of Precision Engineering and Manufacturing-Green Technology, 10*(6), 1605-1613.

**7.** Lee, J., Kim, H.-C., Choi, J.-W. & Lee, I. H. (2017). A review on 3D printed smart devices for 4D printing. *International Journal of Precision Engineering and Manufacturing-Green Technology, 4*(3), 373-383.

**8.** Hossain, M.J., Tabatabaei, B.T., Kiki, M. & Choi, J.-W. (2024). Additive manufacturing of sensors: a comprehensive review. *International Journal of Precision Engineering and Manufacturing-Green Technology.*

**9.** Ko, H., Moon, S.K. & Hwang, J. (2015). Design for additive manufacturing in customized products. *International Journal of Precision Engineering and Manufacturing, 16*(11), 2369-2375.

**10.** Ahn, D.-G. (2016). Direct metal additive manufacturing processes and their sustainable applications for green technology: A review. *International Journal of Precision Engineering and Manufacturing-Green Technology, 3*(4), 381-395.

**11.** Chua, Z.Y., Ahn, I.H. & Moon, S.K. (2017). Process monitoring and inspection systems in metal additive manufacturing: Status and applications. *International Journal of Precision Engineering and Manufacturing-Green Technology, 4*(2), 235-245.

**12.** Kahhal, P., Jo, Y.-K. & Park, S.-H. (2023). Recent progress in remanufacturing technologies using metal additive manufacturing processes and surface treatment. *International Journal of Precision Engineering and Manufacturing-Green Technology.*

**13.** Rosenthal, S., Hahn, M., Tekkaya, A.E., Platt, S., Kleszczynski, S. & Witt, G. (2022). Speeding up additive manufacturing by means of forming for sheet components with core structures. *International Journal of Precision Engineering and Manufacturing-Green Technology, 9*(4), 1021-1034.

**14.** Chu, T., Park, S. & Fu, K. (Kelvin). (2021). 3D printing-enabled advanced electrode architecture design. *Carbon Energy, 3,* 424-439.

**15.** Park, S., Jin, H. & Yun, Y.S. (2020). Advances in the design of 3D-structured electrode materials for lithium-metal anodes. *Advanced Materials, 32,* 2002193.

**16.** Chabi, S., Peng, C., Hu, D. & Zhu, Y. (2014). Ideal three-dimensional electrode structures for electrochemical energy storage. *Advanced Materials, 26,* 2440-2445.

**17.** Arenas, L.F., Ponce De León, C. & Walsh, F.C. (2019). Three-dimensional porous metal electrodes: Fabrication, characterisation and use. *Current Opinion in Electrochemistry, 16,* 1-9.

**18.** Stojić, D. Lj., Marčeta, M.P., Sovilj, S.P. & Miljanić, Š. S. (2003). Hydrogen generation from water electrolysis-possibilities of energy saving. *Journal of Power Sources, 118,* 315-319.

**19.** Rodríguez, J. & Amores, E. (2020). CFD modeling and experimental validation of an alkaline water electrolysis cell for hydrogen production. *Processes, 8,* 1634.

**20.** Fatouh, M., Shedid, M.H. & Elshokary, S. (2013). Effect of operating and geometric parameters on hydrogen production from an alkali electrolyzer. *International Journal on Power Engineering and Energy.*

**21.** Gillespie, M.I. & Kriek, R.J. (2017). Hydrogen production from a rectangular horizontal filter press divergent electrode-flow-through (DEFT™) alkaline electrolysis stack. *Journal of Power Sources, 372,* 252-259.

**22.** González-Buch, C., Herraiz-Cardona, I., Ortega, E., García-Antón, J. & Pérez-Herranz, V. (2016). Study of the catalytic activity of 3D macroporous Ni and NiMo cathodes for hydrogen production by alkaline water electrolysis. *Journal of Applied Electrochemistry, 46,* 791-803.

**23.** Lim, C.W. (2017). Design and manufacture of small-scale wind turbine simulator to emulate torque response of MW wind turbine. *International Journal of Precision Engineering and Manufacturing-Green Technology, 4*(4), 409-418.

**24.** Sung, C.-M. & Han, M.-C. (2016). Design and performance evaluation of hinge type pitch control system in small-size wind turbine. *International Journal of Precision Engineering and Manufacturing-Green Technology, 3*(4), 335-341.

**25.** Kim, S.-H. & Suh, K. (2020). Experimental and numerical investigation on power characteristics of 300 W class horizontal axis wind turbine with wave winding type AFPM generator. *International Journal of Precision Engineering and Manufacturing-Green Technology, 7*(4), 837-848.

**26.** Chen, Y.-J., Huang, G.-Y., Shiah, Y.C. & Tsai, Y.-L. (2020). Performance prediction for small horizontal axis wind turbine (HAWT) by integrated theory and experimental verifications. *International Journal of Precision Engineering and Manufacturing-Green Technology, 7*(1), 131-140.

**27.** Hang, W.X., Tong, C.W., Hoe, W.K., Chin-Tsan, W., Huat, S.L., Chew, P.S. & Hin, L.S. (2018). Preliminary assessment of optimized accessorial roof shape for performance of wind turbine mounted on eco-roof system. *International Journal of Precision Engineering and Manufacturing-Green Technology, 5*(3), 375-385.

**28.** Park, S., Han, G.D., Koo, J., Choi, H.J. & Shim, J.H. (2019). Profitable production of stable electrical power using wind-battery hybrid power systems: a case study from Mt. Taegi, South Korea. *International Journal of Precision Engineering and Manufacturing-Green Technology, 6*(5), 919-930.

**29.** Chi, J. & Yu, H. (2018). Water electrolysis based on renewable energy for hydrogen production. *Chinese Journal of Catalysis, 39,* 390-394.

**30.** Ibáñez-Rioja, A., Järvinen, L., Puranen, P., Kosonen, A., Ruuskanen, V., Hynynen, K., et al. (2023). Off-grid solar PV–wind power–battery–water electrolyzer plant: Simultaneous optimization of component capacities and system control. *Applied Energy, 345,* 121277.

**31.** Kovač, A., Marciuš, D. & Budin, L. (2019). Solar hydrogen production via alkaline water electrolysis. *International Journal of Hydrogen Energy, 44,* 9841-9848.

**32.** Hassan, Q., Sameen, A.Z., Salman, H.M. & Jaszczur, M. (2023). Large-scale green hydrogen production via alkaline water electrolysis using solar and wind energy. *International Journal of Hydrogen Energy, 48,* 34299-34315.

**33.** Belmili, H., Cheikh, R., Smail, T., Seddaoui, N. & Biara, R.W. (2017). Study, design and manufacturing of hybrid vertical axis Savonius wind turbine for urban architecture. *Energy Procedia, 136,* 330-335.

**34.** Shyu, L.S., Lee, C.H., Hsiao, Y.C., Shih, T.M., Chang, C.C. & Wang, D.Y. (2012). High-efficiency 4kW VAWT design and development. *Advanced Materials Research,* 512-515, 617-622.

**35.** Loganathan, B., Chowdhury, H., Mustary, I., Rana, M.M. & Alam, F. (2019). Design of a micro wind turbine and its economic feasibility study for residential power generation in built-up areas. *Energy Procedia, 160,* 812-819.

**36.** Alaskari, M., Abdullah, O. & Majeed, M.H. (2019). Analysis of wind turbine using QBlade software. *IOP Conference Series: Materials Science and Engineering, 518,* 032020.

**37.** Bak, C. (2007). Sensitivity of key parameters in aerodynamic wind turbine rotor design on power and energy performance. *Journal of Physics: Conference Series, 75,* 012008.
**38.** Gupta, A., Abderrahmane, H. A. & Janajreh, I. (2024). Flow analysis and sensitivity study of vertical-axis wind turbine under variable pitching. *Applied Energy, 358,* 122648.
**39.** Jang, H., Hwang, Y., Paek, I. & Lim, S. (2021). Performance evaluation and validation of H-darrieus small vertical axis wind turbine. *International Journal of Precision Engineering and Manufacturing-Green Technology, 8*(6), 1687-1697.
**40.** Rezaeiha, A., Kalkman, I. & Blocken, B. (2017). Effect of pitch angle on power performance and aerodynamics of a vertical axis wind turbine. *Applied Energy, 197,* 132-150.
**41.** Saeidi, D., Sedaghat, A., Alamdari, P. & Alemrajabi, A.A. (2013). Aerodynamic design and economical evaluation of site specific small vertical axis wind turbines. *Applied Energy, 101,* 765-775.
**42.** Seyedzavvar, M. & Boğa, C. (2023). A study on the effects of internal architecture on the mechanical properties and mixed-mode fracture behavior of 3D printed CaCO3/ABS nanocomposite samples. *Rapid Prototyping Journal, 29,* 185-206.
**43.** Seyedzavvar, M. & Boğa, C. (2022). Investigation on the effects of printing pattern on the load carrying capacity of 3D printed U-notched samples. *Meccanica, 57,* 1575-1590.
**44.** Güllü, E., Doğru Mert, B., Nazligul, H., Demirdelen, T. & Gurdal, Y. (2022). Experimental and theoretical study: Design and implementation of a floating photovoltaic system for hydrogen production. *International Journal of Energy Research, 46,* 5083-5098.
**45.** Kaya, M.F., Demir, N., Albawabiji, M.S. & Taş, M. (2017). Investigation of alkaline water electrolysis performance for different cost effective electrodes under magnetic field. *International Journal of Hydrogen Energy, 42,* 17583-17592.
**46.** Koca, M.B., Gümüşgöz Çelik, G., Kardaş, G. & Yazıcı, B. (2019). NiGa modified carbon-felt cathode for hydrogen production. *International Journal of Hydrogen Energy, 44,* 14157-14163.
**47.** Sawadogo Adam, Y., Telli, E., Farsak, M. & Kardaş, G. (2023). Hydrogen production activity of nickel deposited graphite electrodes doped with CoW and CoIr nanoparticles. *International Journal of Hydrogen Energy, 48,* 31844-31854.
**48.** Chakik, F.E., Kaddami, M. & Mikou, M. (2017). Effect of operating parameters on hydrogen production by electrolysis of water. *International Journal of Hydrogen Energy, 42,* 25550-25557.